

Cho, C-G., Kappos, A. J., Moon, H-J. & Lim, H-J. (2015). Experiments and failure analysis of SHCC and reinforced concrete composite slabs. *Engineering Failure Analysis*, 56, pp. 320-331.

doi: 10.1016/j.engfailanal.2015.01.009



**CITY UNIVERSITY
LONDON**

[City Research Online](#)

Original citation: Cho, C-G., Kappos, A. J., Moon, H-J. & Lim, H-J. (2015). Experiments and failure analysis of SHCC and reinforced concrete composite slabs. *Engineering Failure Analysis*, 56, pp. 320-331. doi: 10.1016/j.engfailanal.2015.01.009

Permanent City Research Online URL: <http://openaccess.city.ac.uk/12815/>

Copyright & reuse

City University London has developed City Research Online so that its users may access the research outputs of City University London's staff. Copyright © and Moral Rights for this paper are retained by the individual author(s) and/ or other copyright holders. All material in City Research Online is checked for eligibility for copyright before being made available in the live archive. URLs from City Research Online may be freely distributed and linked to from other web pages.

Versions of research

The version in City Research Online may differ from the final published version. Users are advised to check the Permanent City Research Online URL above for the status of the paper.

Enquiries

If you have any enquiries about any aspect of City Research Online, or if you wish to make contact with the author(s) of this paper, please email the team at publications@city.ac.uk.

1
2 **Experiments and Failure Analysis of SHCC and Reinforced**
3 **Concrete Composite Slabs**
4
5

6 Chang-Geun Cho^{a*}, Andreas J. Kappos^b, Hyung-Joo Moon^c, Hyun-Jin Lim^c
7
8

9 ^a Professor, School of Architecture, Chosun University, Philmundaero 309, Dong-Gu,
10 Gwangju 501-759, Republic of Korea

11 ^b Professor, Dept. of Civil Engineering, City University London, Northampton Square,
12 London, EC1V 0HB, United Kingdom

13 ^c Ph.D Candidate, School of Architecture, Chosun University, Seosuk-Dong 375, Dong-Gu,
14 Gwangju 501-759, Republic of Korea
15

16 * Corresponding author, E-mail: chocg@chosun.ac.kr, Tel: 82-62-230-7023, Fax: 82-62-230-7155,
17 Professor, School of Architecture, Chosun University, Philmundaero 309, Dong-Gu,
18 Gwangju 501-759, Republic of Korea
19
20
21

1 **ABSTRACT**

2

3 For all types of concrete structures, controlling of cracking, as well as the enhancement of

4 serviceability and ultimate flexural capacity are important issues for deck slabs. This study

5 presents an experimental campaign and accompanying nonlinear analysis of a series of Strain

6 Hardening Cementitious Composite (SHCC) and reinforced concrete slab systems,

7 simply-supported and subjected to four-point loading. In order to improve flexural

8 performance both at the service and ultimate limit states, an SHCC layer with thickness of

9 150 to 400 mm was placed on the soffit of the composite slab; the SHCC was manufactured

10 using two different processes, namely cast-in-situ SHCCs and extruded precast SHCC panel.

11 Nonlinear analysis of SHCC and reinforced concrete slabs was also carried out to predict

12 moment and curvature as well as deflections of the slab systems. The developed slab systems

13 were found to have enhanced performance with regard to both at serviceability and flexural

14 capacity, compared to the conventional reinforced concrete slab.

15

16

17 **KEYWORDS**

18

19 Strain-Hardening Cementitious Composite (SHCC); reinforced concrete slab; bending test;

20 flexural analysis; extrusion process; high-ductile tensile strain

21

22

1. Introduction

Strain Hardening Cementitious Composite (SHCC) or Engineered Cementitious Composite (ECC) is a type of composite material consisting mainly from cementitious binders and short polymeric fibres, such as polyvinyl alcohol (PVA) fibres, as shown in Fig. 1 [1-3]. The SHCC was designed to control secondary cracks, increasing tensile stress and fracture energy and hence preventing brittle failure subsequent to the occurrence of the initial flexural cracks [2-6]. The tensile stress-strain behaviour of SHCC is shown in Fig. 2; after initial cracks formed, the tensile stress of the SHCC was sustained until a tensile strain up to 2.0 % was reached [1-4, 6-7]. This is the reason why SHCC exhibits a highly ductile flexural behaviour (shown in Fig. 3) as opposed to plain concrete which is a brittle material in bending [1-4]. The phenomenon that gives rise to this ductility is the inclusion of dispersed short fibres that functioned as bridges between microscopic cracked surfaces of cementitious binder matrix.

Therefore, SHCC is expected to improve the structural performance of concrete members by controlling cracking and deformation, hence allowing longer spans, reducing the amount of required steel bars, and enhancing both the ductility and durability of reinforced concrete members [8-12].

On the other hand, conventional reinforced concrete slab systems are commonly adopted in the design and construction of building structures [13]. However the thickness and the amount of reinforcing bars in such slabs could be reduced if they are made composite by applying profiled steel sheets or high performance composite materials [14-16]. Several types of steel sheet composite slabs were developed and applied in building structures offering advantages in both the construction process and the structural performance [14-16]. High performance materials such as Fibre-reinforced polymer (FRP) composite sheets or bars could also be used

1 to strengthen reinforced concrete slabs, beams, and columns by enhancing their flexural
2 capacity and controlling cracking [17-20].

3 This study reports on experiments and nonlinear analysis carried out to evaluate a series of
4 reinforced concrete composite slabs wherein cast-in-situ SHCCs or extruded precast SHCC
5 panels were used. A series of SHCC and reinforced concrete composite slab specimens was
6 tested; the specimens were simply-supported and subjected to four-point loading, and their
7 response was compared with that of a conventional reinforced concrete slab. The series of
8 specimens were also evaluated using nonlinear analysis, and the structural characteristics of
9 the developed SHCC and reinforced concrete slab systems are discussed herein with focus on
10 their ability to control cracking and enhance the flexural performance.

11 12 13 **2. Nonlinear Flexural Analysis of SHCC and Reinforced Concrete**

14 **Composite Slabs**

15 16 **2.1 Layered approach for flexural analysis of SHCC and reinforced** 17 **concrete sections**

18
19 An inelastic layered approach to predict nonlinear flexural behaviour of SHCC and
20 reinforced concrete sections was formulated as shown in Fig. 4 wherein stress-strain
21 relationships of concrete, reinforcing bars, and SHCC were considered respectively [7, 19].
22 For concrete, the ascending portion was considered as a quadratic function; after reaching its
23 peak, compressive stress follows a linearly descending branch (strain-softening), while

1 concrete in tension is treated as a linear elastic brittle material with stress dropping to zero
 2 subsequent to reaching the tensile strength. The constitutive law adopted for reinforcing bars
 3 was a bilinear one (elastic and strain-hardening branches). The stress - strain relationship for
 4 SHCC was modelled as shown in Fig. 2, i.e. subsequent to tensile cracking, stress was
 5 assumed to remain constant until the tensile strain reaches 0.02, while the compression regime
 6 was modelled similarly to plain concrete in compression. The material properties of concrete,
 7 reinforcing bars, and SHCC used in the nonlinear analysis were based on the results of the
 8 corresponding tests as could be seen in the next section.

9 From the strain profile of a cross-section shown in Fig. 4, the axial strain increment, $d\varepsilon_o$,
 10 could be derived from the resultant axial force increment, dN , and the curvature increment,
 11 $d\phi$, as follows.

$$d\varepsilon_o = (dN - E_M d\phi) / E_N \quad (1)$$

14 where

$$E_N = \left(\sum_{i=1}^{conc} f_{ci} A_{ci} + \sum_{j=1}^{As} f_{sj} A_{sj} + \sum_{k=1}^{SHCC} f_{SHk} A_{SHk} \right) \quad (2)$$

$$E_M = \left(\sum_{i=1}^{conc} f_{ci} A_{ci} z_i + \sum_{j=1}^{As} f_{sj} A_{sj} z_j + \sum_{k=1}^{SHCC} f_{SHk} A_{SHk} z_k \right) \quad (3)$$

18 The nonlinear sectional responses such as the moment-curvature relationship, stresses and
 19 strains in each layer at each stage could be predicted by a layered sectional approach with an
 20 incremental and iterative scheme based on Eq. (1). The analysis was terminated when
 21 compressive strain in a concrete layer reached the ultimate strain (crushing of concrete).

2.2 Prediction of nonlinear load vs. deflection relationship

From the predicted moment vs. curvature curve of the section, three important curvature values, those at initial cracking, ϕ_{cr} , initial yielding of tensile bar, ϕ_y , and ultimate load, ϕ_u , could be found and based on them a multilinear approximation of the d curvature diagram can be drawn. For the standard four-point loading test, the curvature distributions at the aforementioned stages could be estimated by the pertinent three curvatures as shown in Fig. 5. Therefore, the mid-span deflection, Δ_c , at these three stages could be calculated from the moment-area method respectively as follows:

At concrete cracking;

$$\Delta_c = \frac{1}{2}\theta_A L - \phi_{cr} \left[\frac{1}{2}S L_m + \frac{1}{6}S^2 + \frac{1}{2}L_m^2 \right] \quad (4)$$

$$\theta_A = \phi_{cr} \left(\frac{1}{2}S + L_m \right) \quad (5)$$

At yielding of tensile reinforcement;

$$\Delta_c = \frac{1}{2}\theta_A L - \frac{1}{2}\phi_{cr} L_1 \left(L_m + L_2 + \frac{1}{3}L_1 \right) - \phi_{cr} L_2 \left(L_m + \frac{1}{2}L_2 \right) - \frac{1}{2}(\phi_y - \phi_{cr}) L_2 \left(L_m + \frac{1}{3}L_2 \right) - \phi_y L_m \left(\frac{1}{2}L_m \right) \quad (6)$$

$$\theta_A = \frac{1}{2}\phi_{cr} L_1 + \frac{1}{2}(\phi_{cr} + \phi_y) L_2 + \phi_y L_m \quad (7)$$

At ultimate;

$$\Delta_c = \frac{1}{2}\theta_A L - \frac{1}{2}\phi_{cr} L_1 \left(L_m + L_3 + L_2 + \frac{1}{3}L_1 \right) - \phi_{cr} L_2 \left(L_m + L_3 + \frac{1}{2}L_2 \right) \quad (8)$$

$$- \frac{1}{2}(\phi_y - \phi_{cr}) L_2 \left(L_m + L_3 + \frac{1}{3}L_2 \right) - \phi_y L_3 \left(L_m + \frac{1}{2}L_3 \right) - \frac{1}{2}(\phi_u - \phi_y) L_3 \left(L_m + \frac{1}{3}L_3 \right) - \phi_u L_m \left(\frac{1}{2}L_m \right)$$

$$\theta_A = \frac{1}{2}\phi_{cr} L_1 + \frac{1}{2}(\phi_{cr} + \phi_y) L_2 + \frac{1}{2}(\phi_y + \phi_u) L_3 + \phi_u L_m \quad (9)$$

In the above equations, θ_A is the rotation at the support at each loading stage. Therefore, a tri-linear load vs. deflection relationship could be estimated for SHCC and reinforced

1 concrete composite slabs subjected to a standard bending test. It is clear that this procedure is
2 valid when the contribution of both shear deformations and bond slip to the total deflection
3 can be ignored.

4 5 **3. Cast-in-situ SHCC and Reinforced Concrete Composite Slabs**

6 7 **3.1. Details of cast-in-situ slab specimens**

8
9 In this series of composite slabs, flexural performance was improved by controlling
10 cracking at the bottom of the slabs; the specimens were manufactured by casting in-situ an
11 SHCC bottom layer after positioning of longitudinal, transverse, and vertical reinforcing bars
12 and then casting a top layer of normal concrete that constitutes the upper part of the composite
13 slab as shown in Fig. 6. The dimensions of the simply-supported one-way slab specimens, as
14 well as details, diameters, and spacing of reinforcing bars are shown in Fig. 7. For three slab
15 specimens, the span length was 3,400 mm and the thickness of the composite cross-section
16 was 180 mm, with a width of 600 mm. Specimen RC-180 was a conventional reinforced
17 concrete slab, used as a reference specimen, while the two specimens SHCC-20 and
18 SHCC-40 were manufactured as SHCC and reinforced concrete composite slabs, the
19 thickness of the SHCC layer being 20 mm and 40 mm, respectively, as shown in Fig. 8.

20 21 **3.2. Manufacturing of cast-in-situ Slab Specimens**

22
23 Fig. 9 shows the manufacturing process of the slab specimens, i.e. placement of formwork,
24 positioning of reinforcing bars, casting of SHCC, and finally casting of topping concrete. It is

1 noted that to sustain the composite action between the SHCC and the topping concrete,
2 vertical shear reinforcement that crossed the interface was placed, while the top surface of the
3 SHCC layer was roughened 7 days after casting the SHCC. The specimens were cured under
4 wet conditions for four weeks.

5 The SHCC was manufactured using Ordinary Portland Cement (OPC) as the main binder
6 and silica sand as an additive, both of which were made in Korea, and combining with
7 additional admixtures, PVA fibres, and water [4,7,8]. As shown in Table 1, the PVA fibres
8 used as reinforcement of the cementitious binder had a tensile strength of 1,600 MPa, a
9 diameter of 40 μm and a length of 12 mm, and the surface of the fibres was treated using an
10 oiling agent, to improve mixing with cementitious binders [4,7,8]. As for the powdered
11 materials of SHCC, dry mixing was conducted using an omni-mixer and the mixing water
12 was added in two stages for the even distribution of fibres, thus the volumetric ratio of fibres
13 was 2.0 %. Total mixing time was 20 minutes, including 5 minutes of dry mixing, 5 minutes
14 of wet mixing, and 10 minutes of placing.

15 The concrete mix was designed for a uniaxial compressive strength of 30 MPa as shown in
16 Table 2, while the reinforcing bars had a yield stress of 400 MPa [8].

17

18 **3.3. Loading of Slab Specimens**

19

20 Three simply supported slab specimens with a span of 3,400 mm (wherein the pure bending
21 length was 700 mm) were tested under four-point bending using a 1,000 kN UTM actuator.
22 Loading was increased until the specimen was no more able to resist it, as it reached failure
23 by crushing of concrete. The deflection at mid-span was measured using two vertical LVDTs.

1 Curvature was measured with additional four LVDTs attached in the horizontal direction at
2 the bottom and top side of specimens, while strain gauges were attached to top and bottom
3 longitudinal bars near the mid-span with the same spacing as the transverse bars.

4 5 **3.4. Test Results for the Three Specimens**

6
7 At the end of the test, after failure was reached, the three specimens showed crack and
8 failure patterns at mid-span as shown in Fig. 10, while bending moment vs. curvature curves
9 and transverse load vs. deflection curves at mid-span were as shown in Fig. 11 and 12,
10 respectively.

11 In specimen RC-180 the cracks were early initiated near mid-span at a load of 6.6 kN and
12 continued to propagate from mid-span to the support, the spacing of cracks being about
13 100~150 mm. Subsequent to yielding of the longitudinal bars, the width of the existing cracks
14 increased rapidly and they further propagated in the direction of the top surface of the slab
15 until the specimen reached failure. The load was increased up to reaching a deflection of 48.8
16 mm and slightly decreased afterwards. The slab failed at a deflection of 87.5 mm
17 corresponding at a load of 49.5 kN (7.5 times the load at first cracking).

18 In specimen SHCC-20, micro-cracks were observed initially at mid-span at a load of 8.5
19 kN (29% higher than in the reinforced concrete specimen). From that instance up to yielding
20 of reinforcing bars, multiple micro-cracks consecutively formed near the middle of the soffit
21 of the slab but no further opening of cracks was observed and cracking was localised. Due to
22 controlling of multiple micro-cracks, the cracked stiffness of SHCC-20 was found to be
23 higher than that of RC-180. Subsequent to yielding of reinforcing bars, crack opening was
24 restrained to some existing cracks near the mid-span and the specimen continued to resist the

1 transverse load and finally reached failure at a load of 59.8 kN. The specimen SHCC-40 has
2 shown similar trends, i.e. multiple micro-cracking and failure patterns similar to those
3 observed in specimen SHCC-20, and reached failure at a load of 65.2 kN (9% higher than that
4 of SHCC-20).

6 **3.5. Analytical Prediction of the Response of the Specimens**

8 The response of the three slab specimens tested as reported in the previous sections was
9 analysed using the nonlinear analysis model described in section 2. Regarding material
10 characteristics of SHCC, it was assumed that the compressive and tensile strength of SHCC
11 was 31.2 MPa and 3.12 MPa respectively, and the maximum tensile strain was 2.0 %, while
12 after this point the tensile stress dropped to zero as shown in Fig. 2. Material properties of
13 concrete and reinforcing bars were taken from the mechanical tests described in section 3.2.

14 The predicted bending moment vs. curvature and transverse load vs. deflection
15 relationships for the three slabs are shown in Figs. 13 and 14, respectively. As also found in
16 the experimental study, the two specimens SHCC-20 and SHCC-40 show a markedly
17 improved flexural behaviour compared to the reference specimen RC-180, with increased
18 stiffness after cracking as well as enhanced yield and ultimate resistance of the slabs.
19 Comparing Figs. 13 and 14 with Figs 11 and 12, it is seen that for all three specimens, the
20 predicted yielding and failure loads are very close to those found in the experiments, with
21 differences ranging from 0.7% to 2.2%.

4. Extruded SHCC and Reinforced Concrete Composite Slab

4.1. Extrusion of SHCC panel

SHCC can be manufactured using various methods such as cast-in-situ, precast, spray, and extrusion [4, 8-12, 21-22]. SHCC products manufactured using the extrusion process have more reliable mechanical characteristics, i.e. strength, modulus of elasticity, and ductility, which are attributed not only to the mechanical compaction of fresh SHCC caused from the lower porosity after extrusion but also to the aligned orientation of fibres embedded in the cementitious composite [21, 22]. By means of the extrusion process it is easy to manufacture thin and slender precast SHCC panels, which are difficult to achieve using the cast-in-situ method. For mixing SHCC in the framework of the extrusion process, Ordinary Portland Cement (OPC) as the main binder and silica powder as an additive, were used, all made in Korea, to which admixtures and PVA fibres were added, and finally water, following the specified mixing proportions [22]. The PVA fibres used as reinforcement in the cementitious composite binder had a diameter of 39 μm , length of 8mm, and tensile strength of 1,700 MPa [22]. After mixing for about 15 minutes, the fresh SHCC was extruded through a mould which could form the desired shape of the cross-section. Mechanical properties of concrete and reinforcing steel bars were the same as mentioned in the previous sections.

Fig. 15 shows an extruded SHCC panel which was applied to manufacture a specimen of SHCC and reinforced concrete composite slab. To achieve sufficient mechanical characteristics, the curing process of the extruded SHCC panel consisted of two processes, i.e. pre-curing for five hours soon after the extrusion had finished and main curing at 50°C during

1 a period of three days.

3 **4.2. Manufacturing of specimen EXT-P1**

4
5 A specimen of SHCC and reinforced concrete composite slab was manufactured wherein
6 the precast SHCC panel was manufactured by the extrusion process shown in Fig. 15. The
7 SHCC extrusion panel had a thickness of 15 mm and three ribs on its top surface in order to
8 ensure full composite action between the precast SHCC panel and the topping concrete. The
9 height of each rib was 26.5 mm. Fig. 16 shows the dimensions of the cross-section and details
10 of the slab specimen EXT-P1, which has not only the same dimensions and details of
11 reinforcing bars but also the same loading and support conditions in the four-point bending
12 test as the specimens reported in the previous chapter.

14 **4.3. Test results of EXT-P1**

15
16 Fig. 17 shows the cracking and failure patterns of specimen EXT-P1, while moment vs.
17 curvature and mid-span load vs. deflection relationships of the specimen are shown in Fig. 18
18 and 19 respectively; these should be compared with the response of specimen RC-180, the
19 conventional reinforced concrete slab (Figs. 10a, 11, and 12). In specimen EXT-P1, the first
20 crack formed at a load of 7.8 kN on the bottom surface of the SHCC panel near mid-span; this
21 load was slightly lower than the first cracking load in the cast-in-situ specimen SHCC-20. The
22 existing cracks on the surface of extruded SHCC panel did not seem (macroscopically) to
23 open noticeably, but multiple micro-cracks remained until the bending moment reached the
24 value at which yielding of tensile reinforcing bars occurred, at a load of 53.2 kN. As load

1 increased further, multiple micro-cracks propagated extensively on the bottom surface of the
2 SHCC panel as the mid-span deflection reached 29.5 mm, and the specimen showed a stable,
3 strain-hardening, behaviour, having adequate ductility and reaching a maximum load of 63.1
4 kN at a mid-span deflection of 65.7 mm. The specimen finally was failure in flexure at a
5 deflection of 73.0 mm by crushing of concrete at its top. It is notable that prior to failure no
6 signs of debonding and slippage at the interface between the extruded SHCC panel and the
7 topping concrete were observed, but they did appear close to the failure load. Hence, it is seen
8 that the extruded SHCC panel having three ribs on its top surface provided not only sufficient
9 composite action between the SHCC panel and the topping concrete but also adequate control
10 of flexural cracks by developing multiple micro-cracks which prevented the opening and
11 localization of initial cracks that was observed in the reference specimen RC-180. In
12 comparison with the two cast-in-situ slab specimens, SHCC-20 and SHCC-40, specimen
13 EXT-P1, despite its lower thickness of the SHCC layer, showed favourable strain-hardening
14 characteristic in the post-yielding range of its response. The enhanced strain-hardening
15 characteristics of specimen EXT-P1 should be attributed not only to the mechanical
16 compaction of fresh SHCC caused from the lower porosity after extrusion but also to the
17 aligned orientation of fibres embedded in the cementitious composite binder.

18

19 **4.4 Analytical prediction of the response of specimen EXT-P1**

20

21 The response of specimen EXT-P1 was also analysed using the nonlinear model described
22 in section 2. However, in this case due to the need to properly capture the response of the ribs,
23 a grid, rather than a layer, discretization is needed, as shown in Fig. 20. Otherwise, the
24 material characteristics of SHCC and those of the topping concrete and reinforcing bars were

1 considered to be the same as given in the previous sections. Figs. 21 and 22 show the
2 predicted moment vs. curvature and load vs. deflection curves of specimen EXT-P1, to be
3 compared with that of the reinforced concrete slab specimen RC-180. Again, the experimental
4 finding is confirmed that the extruded SHCC and reinforced concrete composite slab shows
5 enhanced flexural performance with improved yield and ultimate loads of the slab compared
6 to the conventional reinforced concrete slab. The predicted yield and ultimate loads for
7 specimen EXT-P1 are 22.9% and 20.1% higher, respectively, compared to the values
8 predicted for specimen RC-180.

9

10 **5. Conclusions**

11

12 In the present study, composite slab systems were introduced that were manufactured by
13 combining cast-in-situ or extruded SHCC panels with a top reinforced concrete layer. From
14 experimental testing and nonlinear analysis of the one-way slab specimens subjected to
15 four-point bending, the following conclusions were obtained.

16 Compared to the reference specimen consisting of a conventional reinforced concrete slab,
17 the composite SHCC and reinforced concrete composite slab systems wherein SHCC with a
18 thickness from 20 to 40 mm was placed at the soffit of the concrete slab gave substantial
19 enhancement in flexural response, increasing post-cracking stiffness as well as yielding and
20 ultimate load capacities of the slabs. This improved performance is attributed to the formation
21 of stable multiple micro-cracks in the SHCC layer as opposed to opening and localization of
22 cracks in conventional reinforced concrete.

23 Comparing the two specimens, SHCC-20 and SHCC-40 that were manufactured with
24 cast-in-situ SHCC, specimen EXT-P1 which was manufactured using an extruded SHCC

1 panel, despite its smaller thickness of the SHCC layer, has shown stable strain-hardening
2 characteristics in the post-yielding range of its response. This performance is attributed not
3 only to the mechanical compaction of fresh SHCC caused from the lower porosity after
4 extrusion but also to the aligned orientation of fibres embedded in the cementitious composite
5 binder.

8 **Acknowledgements**

9
10 The work presented herein was supported by the Basic Science Research Programme
11 through the National Research Foundation of Korea (NRF) funded by the Ministry of
12 Education, Science and Technology (No. 2014044260), and was supported by a grant
13 (14RDRP-B076268) from Regional Development Research Program funded by Ministry of
14 Land, Infrastructure and Transport of Korean government.

16 **References**

- 17
- 18 [1] JSCE. Recommendations for design and construction of high performance fibre
19 reinforced cement composites with multiple fine cracks (HPFRCC). 2008.
- 20 [2] Fischer G, Li VC. Design of engineered cementitious composites (ECC) for processing
21 and workability requirement. Poland: Proceedings of BMC 7 2003; 29-36.
- 22 [3] Lee BY, Cho CG, Lim HJ, Song JK, Yang KH, Li VC, Strain hardening fibre Reinforced
23 alkali-activated mortar - a feasibility study. Construction and Building Materials 2012; 37;

- 1 15~20.
- 2 [4] Choi WC, Yun HD, Cho CG, Feo L. Attempts to apply high performance
3 fibre-reinforced cement composite (HPFRCC) to infrastructures in South Korea.
4 *Composite Structures* 2014; 109; 211-23.
- 5 [5] Herrera-Franco PJ, Valadez-González A. A study of the mechanical properties of short
6 natural-fibre reinforced composites. *Composites Part B: Engineering* 2005;36(8):
7 597-608.
- 8 [6] Wang S, Li VC. Polyvinyl alcohol fibre reinforced Engineered Cementitious Composites:
9 material design and performances. *Proceedings of Int'l RILEM workshop on HPFRCC in*
10 *structural applications*, Published by RILEM SARL; 2006; 65-73.
- 11 [7] Cho CG, Ha GJ, Kim YY. Nonlinear model of reinforced concrete frames retrofitted by
12 in-filled HPFRCC walls. *Struc. Eng. & Mech.*; 2008; 30(2): 211~223.
- 13 [8] Cho CG, Kim YY, Feo L, Hui D. Cyclic responses of reinforced concrete composite
14 columns strengthened in the plastic hinge region by HPFRC mortar. *Composite*
15 *Structures* 2012; 94: 2246-53.
- 16 [9] Kim YY, Lee BY, Bang JW, Han BC, Feo L, Cho CG. Flexural performance of
17 reinforced concrete beams strengthened with strain-hardening cementitious composite
18 and high strength reinforcing steel bar. *Composites: Part B* 2014; 56; 512–19.
- 19 [10] Saje D, Bandelj B, Šušteršič J, Lopati J, Saje F. Autogenous and drying shrinkage of fibre
20 reinforced high-performance concrete. *Journal of Advanced Concrete Technology* 2012;
21 10: 59-73.
- 22 [11] Li M, Li VC. Behavior of ECC/concrete layered repair system under drying shrinkage
23 conditions. *Journal of Restoration of Buildings and Monuments* 2006; 12(2): 143-60.

- 1 [12] Kim YY, Fischer G, Lim YM, Li YC. Mechanical performance of sprayed engineered
2 cementitious composite using wet-mix shotcreting process for repair applications. *ACI*
3 *Materials Journal* 2004; 101(1); 42–49.
- 4 [13] Park R, Paulay, T. Reinforced concrete structures. John Wiley & Sons 1975; 199-203.
- 5 [14] CEN [Comité Européen de Normalisation]. Eurocode 4: Design of composite steel and
6 concrete structures. Part 1-1: General rules and rules for buildings, EN 1994-1-1,
7 Brussels. 2004
- 8 [15] Lopes E, Simoes R. Experimental and analytical behaviour of composite slabs. *Steel and*
9 *Composite Structures* 2008; 8(5); 361-88.
- 10 [16] Salonikios TN, Sextos AG, Kappos AJ. Test on composite slabs and evaluation of
11 relevant Eurocode 4 provisions. *Steel and Composite Structures* 2012; 13(6); 571–586.
- 12 [17] Mitolidis GJ, Salonikios TN, Kappos AJ. Test results and strength estimation of R/C
13 beams strengthened against flexural of shear failure by the use of SRP and CFRP.
14 *Composites: Part B* 2012; 43; 1117–29.
- 15 [18] Cho CG, Kwon M, Spacone E. Analysis model of concrete-filled FRP tubes based on the
16 multi-axial constitutive laws. *Journal of Structural Engineering ASCE* 2005; 131(9);
17 1426-33.
- 18 [19] Cho CG, Kwon M. Prediction of nonlinear bending behavior for FRP concrete beams
19 based on multi-axial constitutive laws. *Engineering Structures* 2008; 30; 2311-20.
- 20 [20] Ha GJ, Cho CG, Kang HW, Feo L. Seismic improvement of RC beam-column joints
21 using hexagonal CFRP bars combined with CFRP sheets. *Composite Structures* 2013; 95;
22 464–70.
- 23 [21] Shao Y, Shah SP. Mechanical properties of PVA fibre reinforced cement composites

1 fabricated by extrusion processing. *ACI Materials Journal* 1997; 94(6); 555–64.
2 [22] Lee BY, Han BC, Cho CG, Kim YY. Flexural performance and fibre distribution of an
3 extruded DFRCC panel. *Computers and Concrete* 2012; 10(2); 105-19.

4

5

Table captions

Table 1. Properties of PVA fibres

Table 2. Mixture design of concrete

Figure captions

Fig.1. PVA fibres and fresh SHCC

Fig.2. Tensile stress-strain curve of SHCC

Fig.3. High flexural deformation of SHCC

Fig.4. Layered flexural model for SHCC and reinforced concrete sections

Fig.5. Linearized curvature distributions at three loading stages

Fig.6. Cross-section of cast-in-situ SHCC and reinforced concrete slabs

Fig.7. Dimensions and reinforcement details for three specimens

Fig.8. Dimensions and reinforcement details in cross-section

Fig.9. Manufacturing process of cast-in-situ SHCC and reinforced concrete slab specimens

Fig.10. Cracks and failure patterns of three specimens

Fig.11. Bending moment vs. curvature curves at mid-span for the three specimens, as found in the experiments

Fig.12. Load vs. deflection curves at mid-span of the three specimens, as found in the experiments

Fig.13. Bending moment vs. curvature curves at mid-span for the three specimens as found from analysis

Fig.14. Load vs. deflection curves at mid-span of the three specimens as found from analysis

Fig.15. An extruded SHCC panel

Fig.16. Cross-sectional details of an extruded SHCC and reinforced concrete slab

Fig.17. Multiple micro-cracks and failure patterns of EXT1-P1

Fig.18. Bending moment vs. curvature curves at mid-span of two specimens, derived experimentally

Fig.19. Load vs. deflection curves at mid-span of two specimens, derived experimentally

Fig.20. Sectional discretization of extruded SHCC and reinforced concrete slab

Fig.21. Bending moment-curvature curves at mid-span of two specimens as derived from analysis

Fig.22. Load vs. deflection curves at mid-span of two specimens, derived from analysis

Table 1. Properties of PVA fibres

Fibre	Density (g/mm ³)	Length (mm)	Diameter (μ m)	Surface Treatment	Tensile Strength (MPa)	Young's Modulus (GPa)	Elongation (%)
PVA	1.3	12	40	Oiling Agent (0.8%)	1,600	39.0	6.0

Table 2. Design of concrete mix

<i>W/C</i> (%)	<i>S/a</i> (%)	Unit weight(kg/m ³)			
		cement	water	Fine aggregate	Coarse aggregate
55.4	49.8	327	181	884	918

W/C: water to cement ratio, *S/a*: sand as percentage of total aggregate



(a) PVA fibre

(b) Fresh SHCC

Fig.1. PVA fibres and fresh SHCC

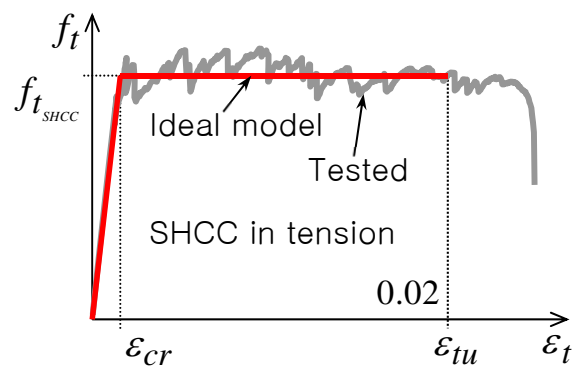


Fig.2. Tensile stress-strain curve of SHCC



Fig.3. High flexural deformation of SHCC

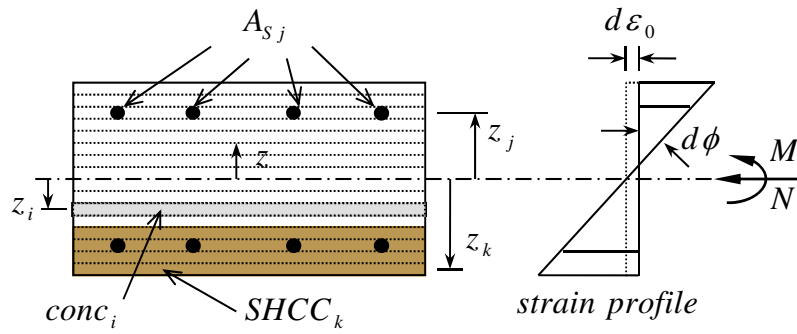


Fig.4. Layered flexural model for SHCC and reinforced concrete sections

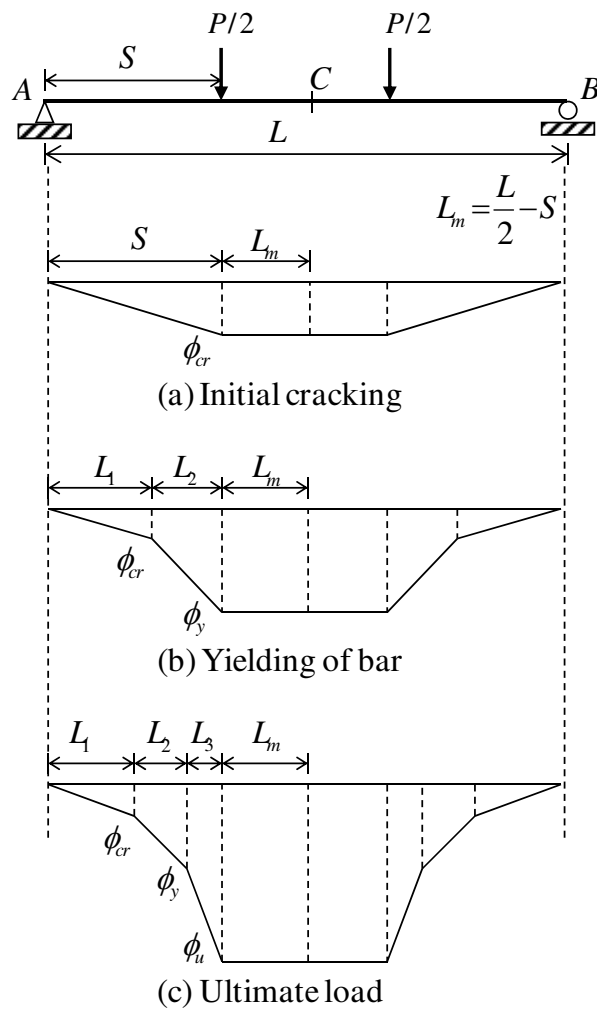


Fig.5. Linearized curvature distributions at three loading stages

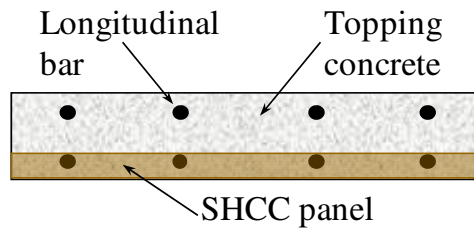


Fig.6. Cross-section of cast-in-situ SHCC and reinforced concrete slabs

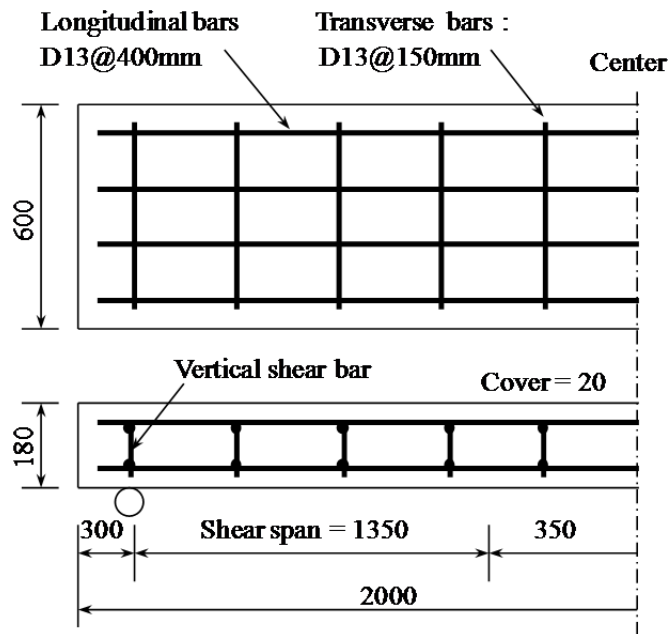


Fig.7. Dimensions and reinforcement details for three specimens

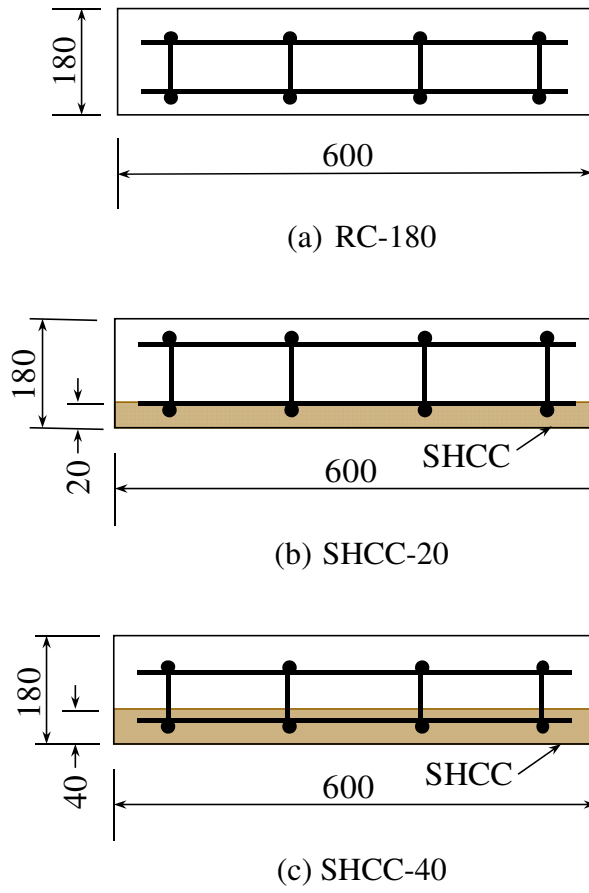
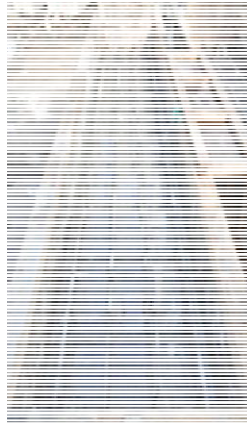


Fig.8. Dimensions and reinforcement details in cross-section



(a) Casting of SHCC

(b) Casting of topping concrete

Fig.9. Manufacturing process of cast-in-situ SHCC and reinforced concrete slab specimens



(a) RC-180



(b) SHCC-20



(c) SHCC-40

Fig.10. Cracks and failure patterns in the three specimens

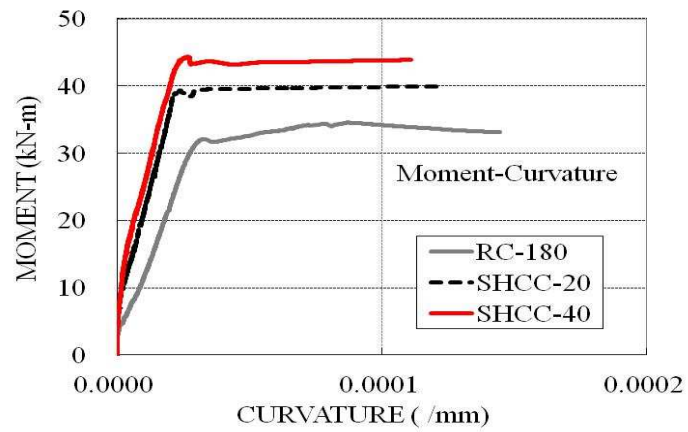


Fig.11. Bending moment vs. curvature curves at mid-span for the three specimens, as found in the experiments

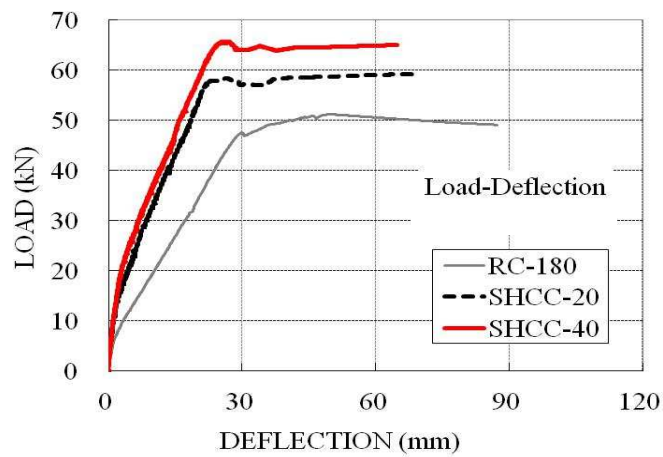


Fig.12. Load vs. deflection curves at mid-span of the three specimens, as found in the experiments

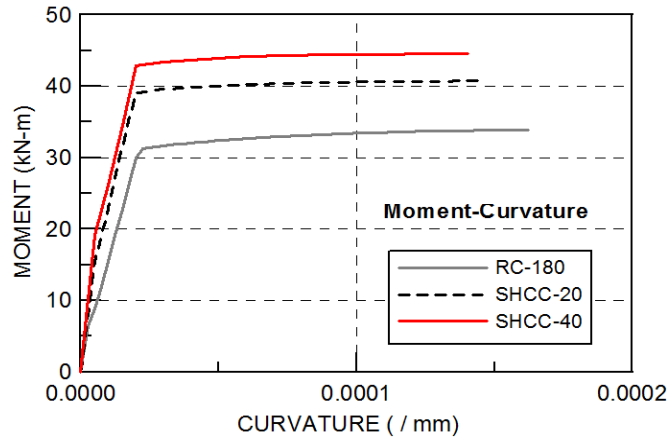


Fig.13. Bending moment vs. curvature curves at mid-span for the three specimens as found from analysis

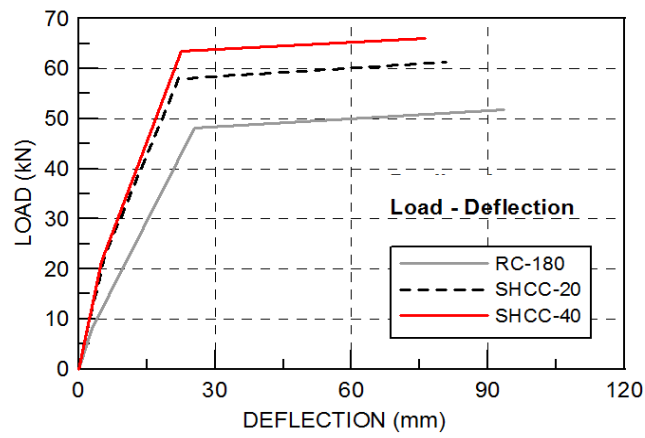


Fig.14 Load vs. deflection curves at mid-span of the three specimens as found from analysis



Fig.15. An extruded SHCC panel

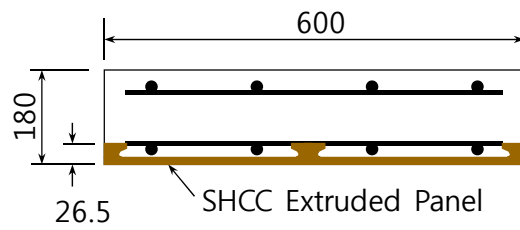


Fig.16. Cross-sectional details of an extruded SHCC and reinforced concrete slab



Fig.17. Multiple micro-cracks and failure pattern of specimen EXT1-P1

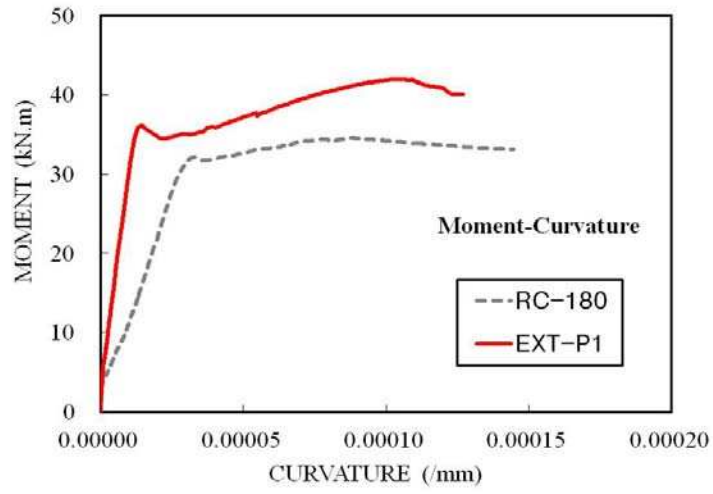


Fig.18. Bending moment vs. curvature curves at mid-span of two specimens, derived experimentally

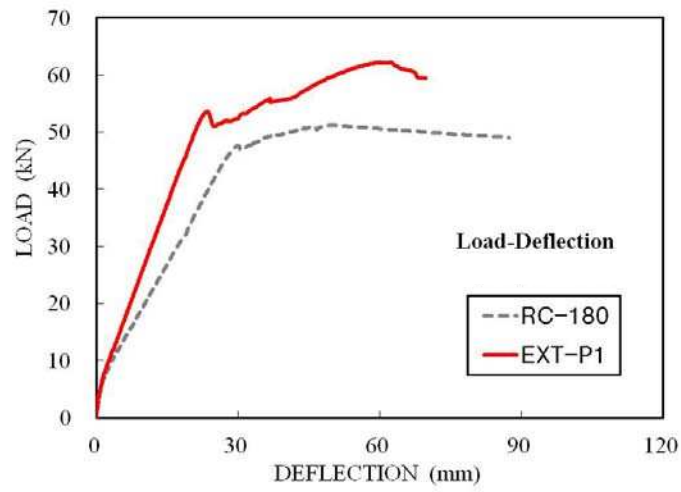


Fig. 19. Load vs. deflection curves at mid-span of two specimens, derived experimentally

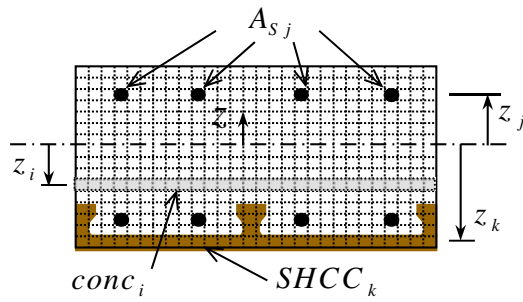


Fig. 20. Sectional discretization of extruded SHCC and reinforced concrete slab

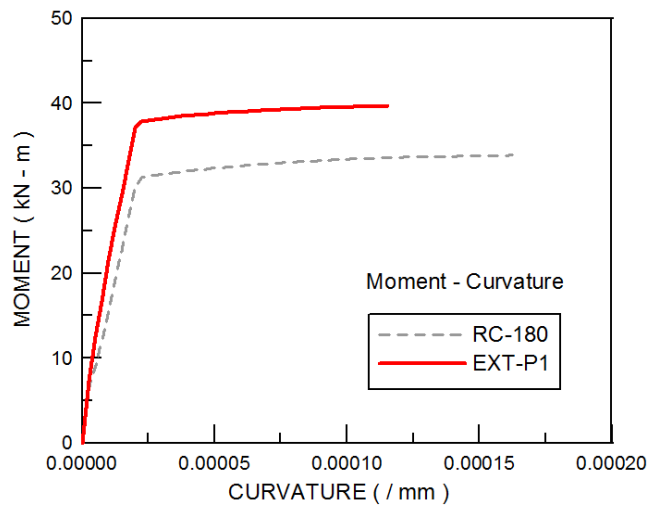


Fig.21. Bending moment vs. curvature curves at mid-span of two specimens as derived from analysis

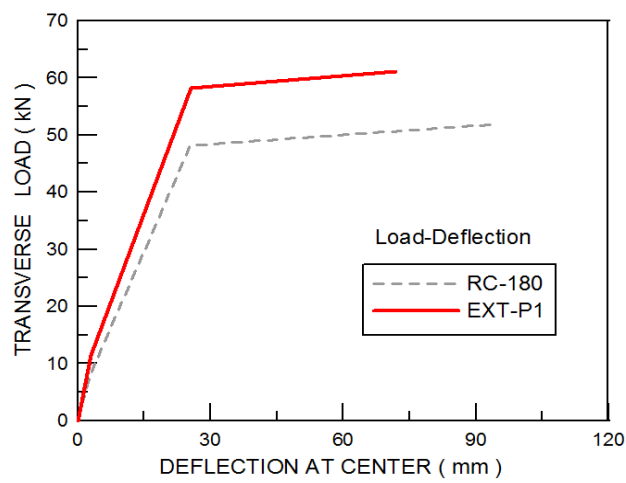


Fig.22. Load vs. deflection curves at mid-span of two specimens, derived from analysis